BASIC SCIENCE

Nanomedicine: Nanotechnology, Biology, and Medicine
48 (2023) 102638

Original Article

nanomedjournal.com

Isolation-free measurement of single urinary extracellular vesicles by imaging flow cytometry

Liang Wu, MD[a,b,*,1], Wouter W. Woud, MSC[a,1], Carla C. Baan, PhD[a], Dennis A. Hesselink, MD, PhD[a], Edwin van der Pol, PhD[c,d,e], Guido Jenster, PhD[f], Karin Boer, PhD[a]

[a]*Erasmus MC Transplant Institute, Department of Internal Medicine, University Medical Center Rotterdam Erasmus MC, 3015GD Rotterdam, the Netherlands*
[b]*Department of Nephrology, The First Affiliated Hospital of Shaoyang University, 422000 Shaoyang, Hunan, China*
[c]*Laboratory Experimental Clinical Chemistry, Amsterdam University Medical Centers, University of Amsterdam, 1007MB Amsterdam, the Netherlands*
[d]*Vesicle Observation Center, Amsterdam University Medical Centers, University of Amsterdam, 1007MB Amsterdam, the Netherlands*
[e]*Biomedical Engineering and Physics, Amsterdam University Medical Centers, University of Amsterdam, 1007MB Amsterdam, the Netherlands*
[f]*Department of Urology, University Medical Center Rotterdam Erasmus MC, 3015GD Rotterdam, the Netherlands*

Revised 1 December 2022

Abstract

Urinary extracellular vesicles (uEVs) are promising biomarkers for various diseases. However, many tools measuring uEVs rely on time-consuming uEV isolation methods, which could induce sample bias. This study demonstrates the detection of single uEVs without isolation using imaging flow cytometry (IFCM). Unstained urine samples contained auto-fluorescent (A-F) particles when characterized with IFCM. Centrifugation successfully removed A-F particles from the unprocessed urine. Based on the disappearance of A-F particles, a gate was defined to distinguish uEVs from A-F particles. The final readouts of IFCM were verified as single EVs based on detergent treatment and serial dilutions. When developing this protocol to measure urine samples with abnormally high protein levels, 25 mg/mL dithiothreitol (DTT) showed improved uEV recovery over 200 mg/mL DTT. This study provides an isolation-free protocol using IFCM to quantify and phenotype single uEVs, eliminating the hindrance and influence of A-F particles, protein aggregates, and coincidence events.

Keywords: Extracellular vesicles; Imaging flow cytometry; Isolation-free methodology; Human urine; Kidney transplantation

Introduction

Extracellular vesicles (EVs) are phospholipid bilayers widely released by cells into body fluids, such as blood and urine. Their reported size ranges from 30 nm to 8000 nm, with most EVs <200 nm.[1–3] EVs reflect parental cell status via variations in EV concentration, composition, or cargo and are considered minimally invasive biomarkers.[1]

Urinary extracellular vesicles (uEVs) are ideal biomarkers as urine collection is non-invasive and easily repeated.[4] uEVs show meaningful values in diagnosing renal and urinary system diseases,[5–7] and illnesses of other systems, such as Parkinson's disease and liver cirrhosis.[8,9]

Despite the perspective as a clinical marker, uEV quantification and characterization are hampered because of their small size, urine contaminants, and lack of methods for accurate detection.[1,10] Nanoparticle tracking analysis (NTA), resistive pulse sensing (RPS), and flow cytometry (FCM) are the most commonly used single-EV-quantification techniques.[1] However, NTA and RPS are limited in phenotyping capabilities, struggling to distinguish uEVs from other particles, such as protein aggregates.[1,11] Although some modern flow cytometers can detect small EVs (<100 nm) based on light scattering, most flow cytometers in clinical research labs have a size detection limit of >600 nm.[12] Moreover, some particles in urine emit autofluorescence, leading to false-positive signals in FCM, regardless of

* Corresponding author at: Room No. Na-514, Erasmus MC Transplant Institute, Department of Internal Medicine, University Medical Center Rotterdam Erasmus MC, Doctor Molewaterplein 40, 3015 GD Rotterdam, the Netherlands.
E-mail address: l.wu.1@erasmusmc.nl (L. Wu).
[1] These authors contributed equally to this work.

https://doi.org/10.1016/j.nano.2022.102638

Please cite this article as: Wu L, et al, Isolation-free measurement of single urinary extracellular vesicles by imaging flow cytometry. *Nanomedicine: NBM* 2023;48:102638, https://doi.org/10.1016/j.nano.2022.102638

labeling.[13,14] The origin of these autofluorescent (A-F) particles is still unclear and how to distinguish them from uEVs needs more research. The direct measurement of uEV is also hampered by Tamm-Horsfall protein (THP), a highly abundant urinary protein, easily entrapping uEVs.[13–16]

Due to the limitations of traditional techniques and the complex composition of urine, uEV purification is commonly required before detection.[17] However, no (combination of) isolation methods, including ultracentrifugation, ultrafiltration, precipitation, or size exclusion chromatography, can reach 100 % uEV purity and yield due to significant loss of uEVs or co-isolation of other particles.[1,17] Some purification procedure likely alters uEV properties.[14,18–20] Ultrafiltration can disintegrate large EVs to generate smaller particles, misunderstood as natural EVs.[18] Ultracentrifugation might cause EV aggregation and encapsulation of multiple small uEV inside bigger uEV.[14,19,20]

Endowed with increased fluorescence detection sensitivity over conventional FCM,[21] and the capability of distinguishing particles based on high-resolution imaging,[22] imaging FCM (IFCM) allows quantification and characterization of uEVs to solve the mentioned difficulties and bypass EV isolation. IFCM has been demonstrated for single EV measurement in minimally processed plasma[23], cell supernatant,[22] and isolated uEVs,[24,25] but no methodology to detect uEVs from urine without relying on prior EV purification. The current study aims to provide a protocol to characterize uEVs by IFCM directly in stained urine by excluding A-F particles and diminishing the influence of THP.

Material and methods

Urine samples were measured by (1) transmission electron microscopy (TEM), (2) nanoparticle tracking analysis (NTA), (3) time-resolved fluorescence immunoassay (TR-FIA), and (4) IFCM without using any uEV isolation method. Supernatant harvested from COLO-205 cells was used as a positive control to investigate the inter- and intra-assay reproducibility during IFCM measurement. TEM, NTA, and TR-FIA protocols were introduced in supplementary materials, including the COLO-205 cell culturing, the measurement of urine protein, creatinine, pH, Tamm-Horsfall protein, and urine treatment with dithiothreitol (DTT).

Collection of urine samples

Urine was collected from 5 healthy controls (HC; Medical Ethical Review number 2018–1623) and 5 kidney transplant recipients (KTR) with acute kidney injury in the first 2 weeks post-transplantation (Medical Ethical Review number 2018–035), approved by the institutional review board of the Erasmus MC. Details regarding the collection of urine samples were demonstrated in the Supplementary material. The gender, age, pH, urinary total protein concentration, and urine creatinine concentration of included individuals are shown in Supplementary Table S1.

Labeling EVs from urine for IFCM

CD9 and CD63 are tetraspanins playing critical roles in EV generation and excretion.[26] Both are used as general uEV surface markers.[27] Urine and COLO-205 cell medium (positive control) were stained with antibodies (all from Biolegend, USA): CD63-Alexa488 (clone H5C6; fluorophore-to-protein ratio 5.20); CD63-APC (clone H5C6; fluorophore-to-protein ratio 1.22); IgG1-Alexa488 or IgG1-APC (both clone MOPC-21). Our study aims to investigate diverse uEV populations by combining markers conjugated with different fluorophores, so two CD63 antibodies were used to demonstrate the influence of fluorophore conjugation on the uEV-IFCM detection and compare the single- and double-positive backgrounds. Antibodies (100–200 μL) were centrifuged at 16,000 *g* at 4 °C for 10 min (FrescoTM 17 Microcentrifuge, Thermofisher Scientific), and only the supernatant was pipetted to avoid aggregates. Based on titration, the final concentration of all antibodies in the sample solution was 0.44 μg/mL. 112 μL of samples were incubated with 4 μL of 15-fold-diluted CD63-Alexa488 and 4 μL of 15-fold-diluted CD63-APC at 4 °C in the dark overnight (dilution by 0.2-μm-pore-filtered Dulbecco's phosphate-buffered saline; fDPBS). IgG1-Alexa488 and IgG1-APC were used as isotypes. The stained sample was treated with 6 μL of 10 % (v/v) Triton-X-100 at room temperature for 30 min to lyse biological structures, such as EVs.

Acquisition settings of ImageStream^x MkII

Multispectral IFCM was performed using Amins ImageStream *MKII* (ISx, Luminex, Seattle, WA, USA), with data acquisition by software INSPIRE® (version: 200.1.681, EMD Millipore). INSPIRE® runs a quality control procedure with built-in ASSIST® as the daily startup procedure. The settings of INSPIRE® in the acquisition: low-speed (velocity: 40 mm/s) & high sensitivity, 6 μm core diameter, 60× magnification, 488-nm laser power at channel 02 (Ch02) detecting Alexa488: 200 mW; 642-nm laser power at channel 05 (Ch05) detecting APC: 150 mW, 1.25 mW laser power at channel 06 (Ch06) detecting side scatter (SSC), and activated channel 04 (Ch04) for detection of bright field. To monitor sample flow and maintain the camera's focus in ISx, polystyrene speed beads (catalog no. 400041, Luminex) were loaded together with samples at 15 %. Each acquisition lasted 180 s, the "Prime" function was clicked once for loading samples fast, and "Remove Speed Beads" was unchecked to maintain speed beads during acquisition.

IFCM analysis

Raw image files acquired from INSPIRE® were analyzed by ISx Data Exploration and Analysis Software (IDEAS® 6.2, EMD Millipore).

"Masks" define a specific area within images to select and quantify pixels. Masks in Ch01 to Ch06 pictures were labeled from M01 to M06, and Mask Combined (MC) includes M01 to M06. Different functions can be applied to each Mask to adjust the position and region of selected pixels. Mask with the "Intensity" function contains pixels showing higher intensity than the backgrounds. The Mask with the "Peak" function (model: Bright) identifies the brightest pixels with the peak intensity in each event, designed for fluorescent spot recognition.[28] The intensity threshold of the Peak Mask is determined by its cell-to-

background ratio. The name of M02 in Ch02, with Peak function, Bright model, and cell-to-background ratio 1, is simplified as Peak (M02, Ch02, Bright, 1). Masks, Peak (M02, Ch02, Bright, 1), and Peak (M05, Ch05, Bright, 1) were used to include the pixels of Alexa488+ and APC+ fluorescent spots. By using the Boolean logic function, Peak masks applied for Ch02 and Ch05 were combined as "Peak (M02, Ch02, Bright, 1) OR Peak (M05, Ch05, Bright, 1)".

"Feature" is further applied upon Mask to analyze quantitative and positional information of selected pixels. Mask selection significantly influences feature characteristics because Mask determines the region of analysis for any given Feature.[28] Hence, the combination of Feature and Mask is instrument/analysis-specific and independent of the sample. Intensity MC is designed to match Intensity Feature for quantifying fluorescence in Ch02, Ch03, Ch05, or SSC signals in Ch06. We chose Peak Masks (M02, Ch02, Bright, 1) and (M05, Ch05, Bright, 1) to be combined with "Spot Count Ch02" and "Spot Count Ch05" features, respectively, because Peak Mask can sensitively recognize fluorescent spot numbers in Ch02 and Ch05.[22,28] Distance between spots presented in a single event but different channels can be analyzed after combining Masks in those channels. The feature "Spot Distance Min" was applied on the composite mask "Peak (M02, Ch02, Bright, 1) OR Peak (M05, Ch05, Bright, 1)" to measure the minimal distance between Alexa488+ and APC+ spots within an image.[23] When this value of "Spot Distance (Ch02 & Ch05)" was 0, the positions of Alexa488+ and APC+ particles overlapped.[23]

An analysis template that summarizes all used features and accompanying masks can be found in Supplementary Table S2.

Calibration of the IFCM

Size-related calibration was performed by measuring SSC of beads of known diameter and refractive index (Gigamix, BioCytex, The Netherlands) followed by Mie theory using the scripts of Rosetta Calibration (v1.29, Exometry, The Netherlands).[29] EVs were modeled as core-shell particles with a core refractive index of 1.38, a shell refractive index of 1.48 and a shell thickness of 6 nm. The calibration based on SSC using Gigamix and Rosetta Calibration has previously been reported by our team using the same machine and acquisition settings.[23]

Calibration of the fluorescence intensity was based on three Quantum™ MESF (molecules of equivalent soluble fluorochrome) kits containing four populations of beads with varying amounts of Alexa488, APC, or PE (Bangs Laboratories, USA).[25] For each kit, the median fluorescence intensity (MFI) of beads was measured by IFCM and converted into MESF based on the instructions of the manufacturer (https://www.bangslabs.com/quickcal). Data was presented in Supplementary Table S3 & Fig. S1. The regression coefficient values for each fluorochrome (R^2-Alexa488: 0.9987; R^2-PE: 0.9948; R^2-APC: 0.9955) indicated that obtained MFI could be readily converted into MESF values.

EV-Track

Experimental details have been uploaded to the EV-TRACK (ID: EV220008), an open-access knowledgebase recommended by the International Society for Extracellular Vesicles to track worldwide EV research.[1,30]

Statistical analysis

GraphPad Prism 8.0 (GraphPad Software, USA) was used to analyze and visualize the data. Data were presented as mean ± standard deviation. In the calibration of MESF in IFCM, the analysis templates calculated the correlation coefficient (R^2) values between MFI and MESF. The coefficient of variation (CV) reflected the reproducibility of IFCM. Paired t-tests were used to show the differences in uEVs numbers or urinary pH between urine samples with different treatments. Unpaired t-tests were utilized to show the differences in urinary protein levels between HCs and KTRs. Linear regression analysis demonstrated the association between IFCM and TR-FIA readouts. Statistical significance was defined by p-values <0.05 (two-tailed).

Result

Outline of the manuscript

The workflow of this study is schematically summarized in Fig. 1. We aimed for a standardized uEV-IFCM measurement independent of uEV purification for clinical usage. To this end, supporting techniques (TEM, NTA, TR-FIA) were used to indicate the size distribution, concentration, and markers of uEVs in the unprocessed urine. The IFCM machine was calibrated with standardized reference material for cross-platform comparisons and then used to phenotype and characterize uEVs in the minimally processed urine (unprocessed urine with labeling). Urine samples from healthy controls (HC) were initially used to establish the uEV-IFCM protocol, which was further developed using the urine of kidney transplant recipients (KTR).

Measuring uEVs by TEM, NTA, and TR-FIA

In HC urine samples imaged by TEM, uEV-like cup-shaped structures were observed with diameters between 50 and 100 nm (Fig. 2A, large-area images in Supplementary Fig. S2). With NTA, we summarized the single-particle-size reports from all HC urine samples. We found that 93–98 % of urine particles' diameter was <400 nm, but 2–7 % of all detected particles showed a size from 400 nm to 1200 nm (Fig. 2B). The total concentration of particles measured by NTA was around 10^8/mL, which is an order of magnitude estimate of particles exceeding the lower limit of detection (LoD).[31] We estimate the LoD to be ~90 nm based on the distribution mode.

To select appropriate labeling for detecting uEV by IFCM, we compared the relative expression levels on uEVs using TR-FIA. In Fig. 2C, CD63 was 6.7-fold higher than CD9 following the Europium intensity ($p = 0.0302$), corresponding with previous research.[32] Hence, CD63+ uEV was chosen as a targeted population to demonstrate the following isolation-free uEV-IFCM methodology.

Gating strategy identifying CD63+ uEV singlets

Standardize the range of detected uEV size

After knowing the size range and marker of uEV in the unprocessed urine samples, a step-by-step gating strategy was developed

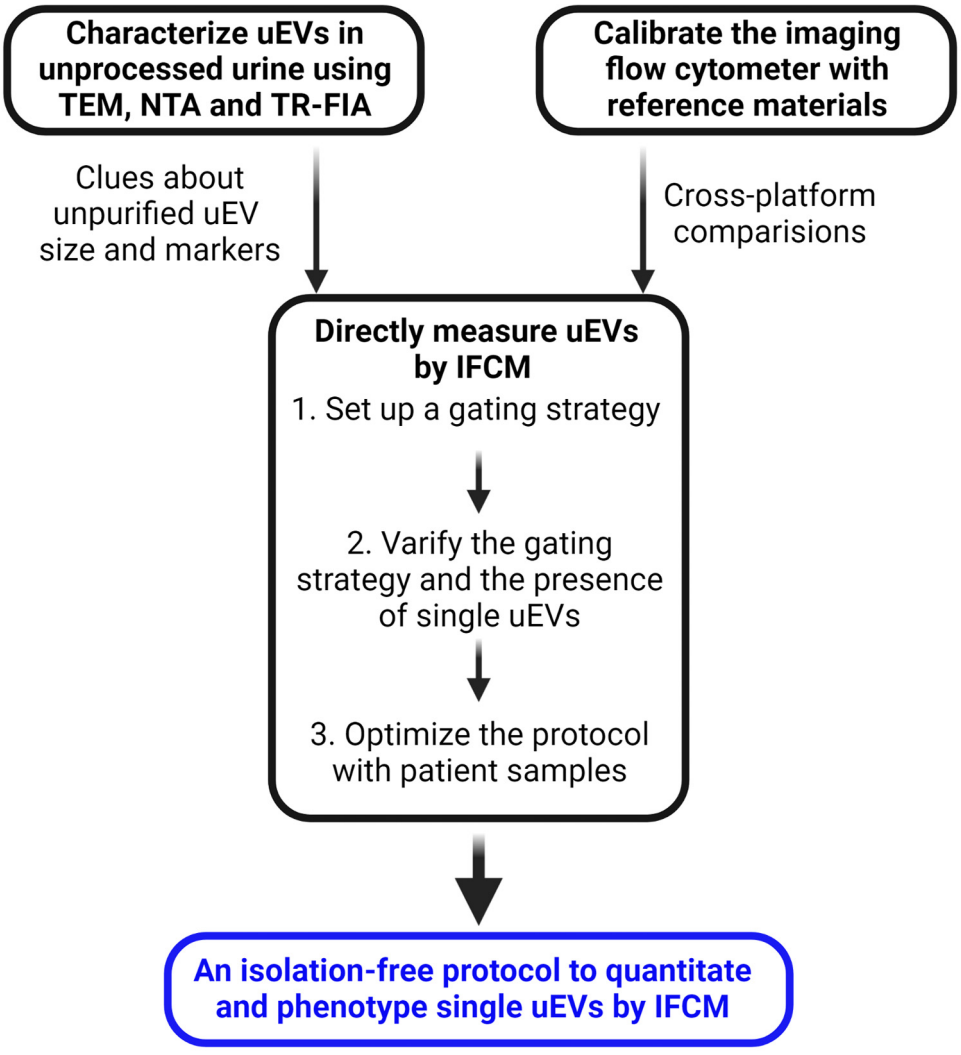

Fig. 1. Schematic workflow of this study.

to distinguish single CD63+ uEV particles from non-uEV components or coincidence events in IFCM.

As demonstrated with NTA (Fig. 2B), we chose the detection range of <1200 nm to include virtually all uEVs. Based on the previously published calibration of our IFCM, an SSC cutoff value of 5279.179 arbitrary units, corresponding to 1200-nm diameter EVs, was obtained and used to include uEVs ≤1200 nm for all the following analyses.[23]

Exclude multiplets and false singlets

The fluorescence intensity of uEVs in multiplets cannot be individually characterized.[28] Following previous research, we also initially tried to utilize the masks with the "Intensity" function to calculate the spot count feature.[22,23] However, the Intensity Mask mistook close doublets as singlets (Supplementary Fig. S3A). Compared to Intensity Mask, Peak Mask only selects pixels with peak intensity (Supplementary Fig. S3B).[28] Therefore, the spot numbers could be more precisely calculated using the Peak Mask than the Intensity Mask. The spot-to-background ratio of the Peak Mask should not be higher than the value of 1. Otherwise, spot counts are underestimated. When the ratio was 3, this Peak mask ignored pixels with <3-fold of the average intensity of the whole image, leading to missing dim spots (Supplementary Fig. S3C). Notably, "<1" of this ratio has no meaning because in the Peak mask with the bright model, the intensity of included pixels must be higher than the background.[28] Hence, the Peak Mask with a spot-to-cell background ratio of 1 was the most appropriate for identifying singlets and excluding events with >1 spot in fluorescence-detecting channels (Ch02 & Ch05). The next step, coincidence/false "singlets" (one green and one red object, but their positions did not overlap), were excluded based on the distance between Ch02 and Ch05 spots ≠ 0.

Distinguish uEV singlets from auto-fluorescent particles in the stained urine

Fluorescent events were detected in all unprocessed urine samples (no staining). In fDPBS, no positive particles (Fig. 3A)

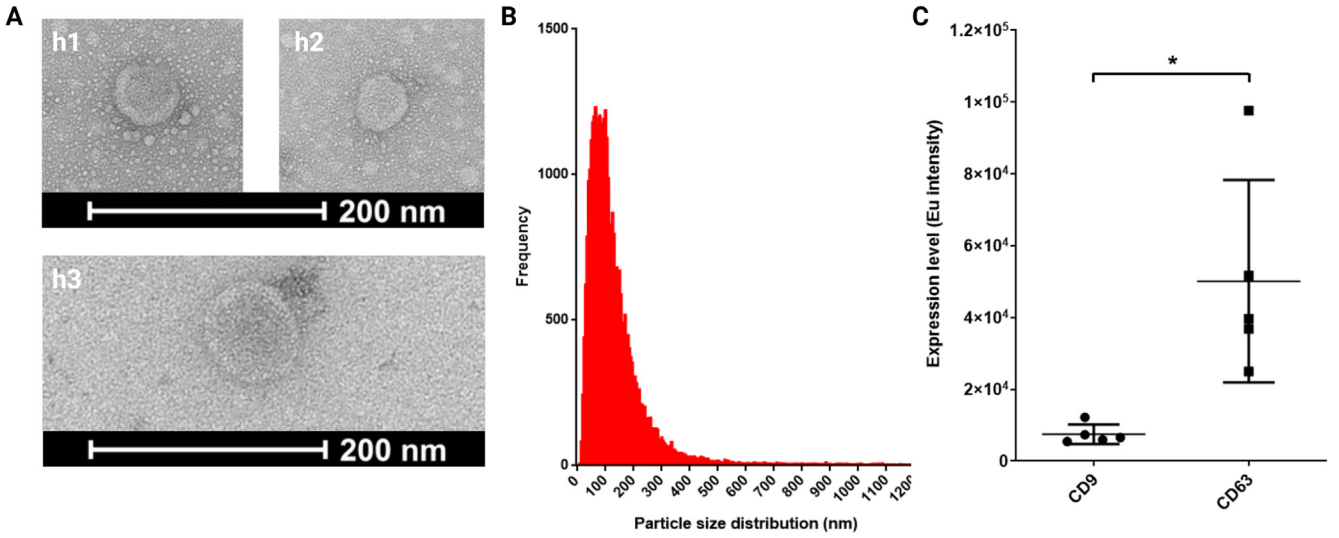

Fig. 2. uEV characteristics tested by TEM, NTA, and TR-FIA in the HC urine (n = 5). (A) uEV-like structures in TEM. (B) The size distribution of urinary particles in NTA. (C) uEV tetraspanin levels tested by TR-FIA. *$p < 0.05$.

were observed. Conversely, unprocessed urine (without staining) contained $1.6 \pm 0.7 \times 10^6$ objects/mL positive particles (Fig. 3B). These events are auto-fluorescent (A-F) particles and demonstrated positive fluorescent signals in fluorescence-detecting channels: Ch02, Ch03, and Ch05. Ch02 and Ch05 were used to detect Alexa488, and APC signals, respectively. No fluorescent reagent was used for Ch03, so it only presented the A-F signals. In the minimally processed urine (urine only with labeling), the distribution of A-F particles overlapped with positive uEVs (Fig. 3C), necessitating the exclusion/removal of A-F particles. Lowering laser power or detergent treatment did not sufficiently remove A-F particles (Fig. 3D). Hence, these A-F particles are not phospholipid bilayer structures, and their A-F signal is unrelated to the high laser power. A step of short-run centrifugation (10,000 $g \times 10$ min) was found to remove 98.9 ± 0.3 % of A-F particles ($p = 0.0058$; Fig. 3D).

Though centrifugation effectively removed A-F particles, it could cause a loss of uEVs. We designed a gating strategy distinguishing non-A-F particles (uEVs) from A-F particles based on the absence of A-F particles in centrifuged urine and aimed to bypass centrifugation finally. First, urine was "cleaned" using that centrifugation (Fig. 3B–E). Next, centrifuged urine was stained with CD63-Alexa488 and CD63-APC to show positive uEVs (Fig. 3F). The spillover from Ch02 to Ch03 was compensated (value: 0.19 in the compensation matrix), so uEVs were horizontally distributed in Fig. 3G. Notably, applying this compensation to A-F particles in the unprocessed urine did not alter the A-F signal (Supplementary Fig. S4). Based on the remaining events after this centrifugation, a gate, "Non-A-F Particles", was set in Ch03 with a cutoff value of 150 A-F intensity (arbitrary unit), which is equal to 5 MESF-PE (blue gate in Fig. 3G). Then, the obtained compensation matrix and gate were applied to urine samples without centrifugation (blue gate in Fig. 3H). By doing so, A-F particles were excluded from the following analysis without requiring centrifugation, and therefore, urine was kept minimally processed until uEV labeling, thus bypassing potential uEV loss. The "Non-A-F Particles" gate was permanently applied to distinguish non-A-F particles from A-F particles in all the following uEV-IFCM analyses (Supplementary Fig. S5). Typical images of distinguished positive uEVs and excluded A-F particles were presented in Fig. 3I.

Detect fluorescently labeled uEV singlets

The next step is to distinguish single-positive and double-positive uEVs. The cutoff fluorescent intensity of APC −/+ was established by staining samples with CD63-Alexa488 and isotype (IgG1)-APC. Based on the APC threshold, we set up the green gate in Supplementary Fig. S6B to include the Alexa488-single-positive uEVs. Likewise, the Alexa488 −/+ cutoff value was set by staining urine with IgG1-Alxea488 and CD63-APC and then obtaining the red gate in Supplementary Fig. S6C for APC-single-positive uEVs. By doing so, spillover between Ch02 and Ch05 was compensated. Alexa488 −/+ threshold intensity was 22 MESF-Alexa488, and the APC one was 1463 MESF-APC. After combining them, double-positive uEVs were separated from other populations and gated in the blue region in Supplementary Fig. S6D. These thresholds were established based on multiple urine samples without gating differences observed, indicating that these gates can be repeatedly applied.

Here, we summarized the logic of the whole IFCM gating strategy (Fig. 4). After excluding A-F particles, the analysis of double-CD63-stained HC urine samples demonstrated three uEV populations as the final readout: CD63-Alexa488 single-positive, CD63-APC single-positive, and double-positive uEV singlets.

Verification of gating strategy and uEV presence

Background analysis

Without performing any wash steps, it was essential to verify the presence of CD63+ uEVs by showing the background of our protocol.

First, detergent treatment was used to check if the readouts of IFCM represent biological membrane structures. Before detergent treatment, for all HC urine samples (double-CD63-stained),

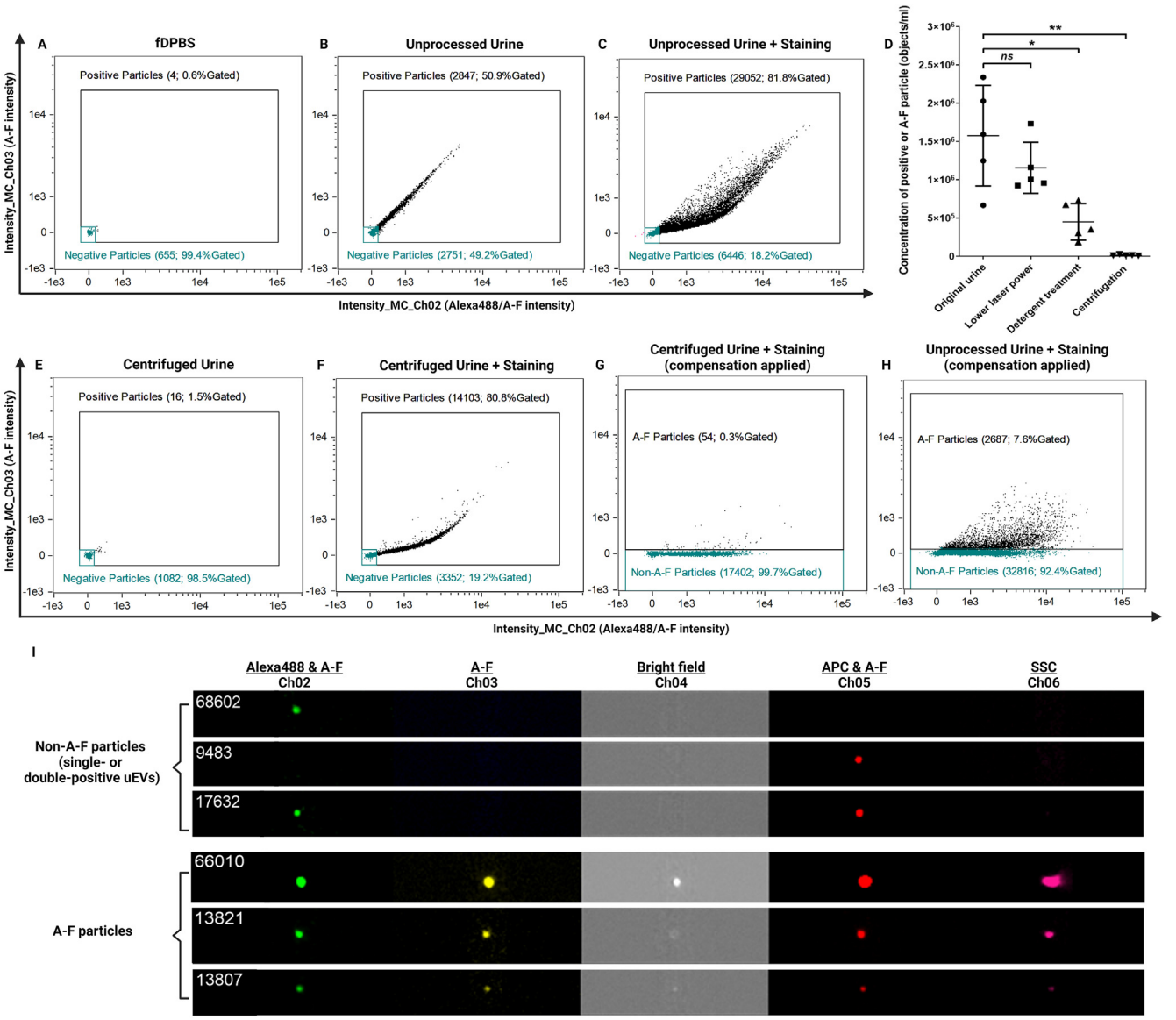

Fig. 3. Distinguish non-A-F particles/uEVs from A-F particles in the stained urine using IFCM. No compensation in A-C, E, F. Based on fDPBS (A), the gates "Negative Particles" and "Positive Particles" were established and applied to present A-F particles in the unprocessed urine (B). (C) A-F particles and positive uEVs could not be distinguished in urine with double-CD63 staining. (D) Methods for removing A-F particles in unprocessed urine (n = 5). "Original urine": unstained urine without any treatments. Compared to the control, the "Lower laser power" group used a quarter of the laser voltage of Ch02 and Ch05; "Detergent treatment" was incubated with 2.0 % TritonX-100 at room temperature for 30 min; "Centrifugation" was centrifuged at 10,000 *g* for 10 min and removed the pellet. $^{**}p < 0.01$; $^{*}p < 0.05$; ns, no significance. (E) The absence of A-F particles in the urine supernatant after centrifugation (10,000 *g* 10 min). (F) Centrifuged urine was CD63-stained to present the distribution of non-A-F particles (uEVs). (G) A compensation matrix was applied in (F) to eliminate spillovers between Ch02 and Ch03, and the gate "Non-A-F Particles" was set up. (H) The compensation matrix and the gate "Non-A-F Particles" were applied to the CD63-stained urine (no centrifugation). (I) Typical images of positive uEVs and A-F particles in double-CD63-stained urine.

we found that the majority of readouts were "++" particles, 3.8 ± 1.3 × 10^7 objects/mL (Fig. 5A). After detergent treatment, "++" events decreased to 4.8 ± 2.7 × 10^5 objects/mL, representing a 98.5 ± 0.9 % decrease compared to no detergent ($p = 0.0034$). As for the single-positive particles in the stained urine, 3.2 ± 2.5 × 10^6 objects/mL of events were "CD63-Alexa488+" (Fig. 5B), and 5.8 ± 0.6 × 10^5 objects/mL of events were "CD63-APC+" (Fig. 5C). After detergent treatment, the concentration of the single "CD63-Alexa488+" events and the "CD63-APC+" events was reduced by 91.3 ± 6.7 % and 77.9 ± 30.1 %, respectively (Fig. 5B & C).

Next to detergent treatment, the double-positive concentrations in other controls were summarized in Fig. 5A. Compared with unstained, isotype-stained, and double-stained plus detergent-treated urine, the average uEV-to-background concentration ratio for the double-positive region in double-stained urine is 3102.2-fold, indicating a convincing presence of CD63+ uEVs in the minimally processed urine. Compared to

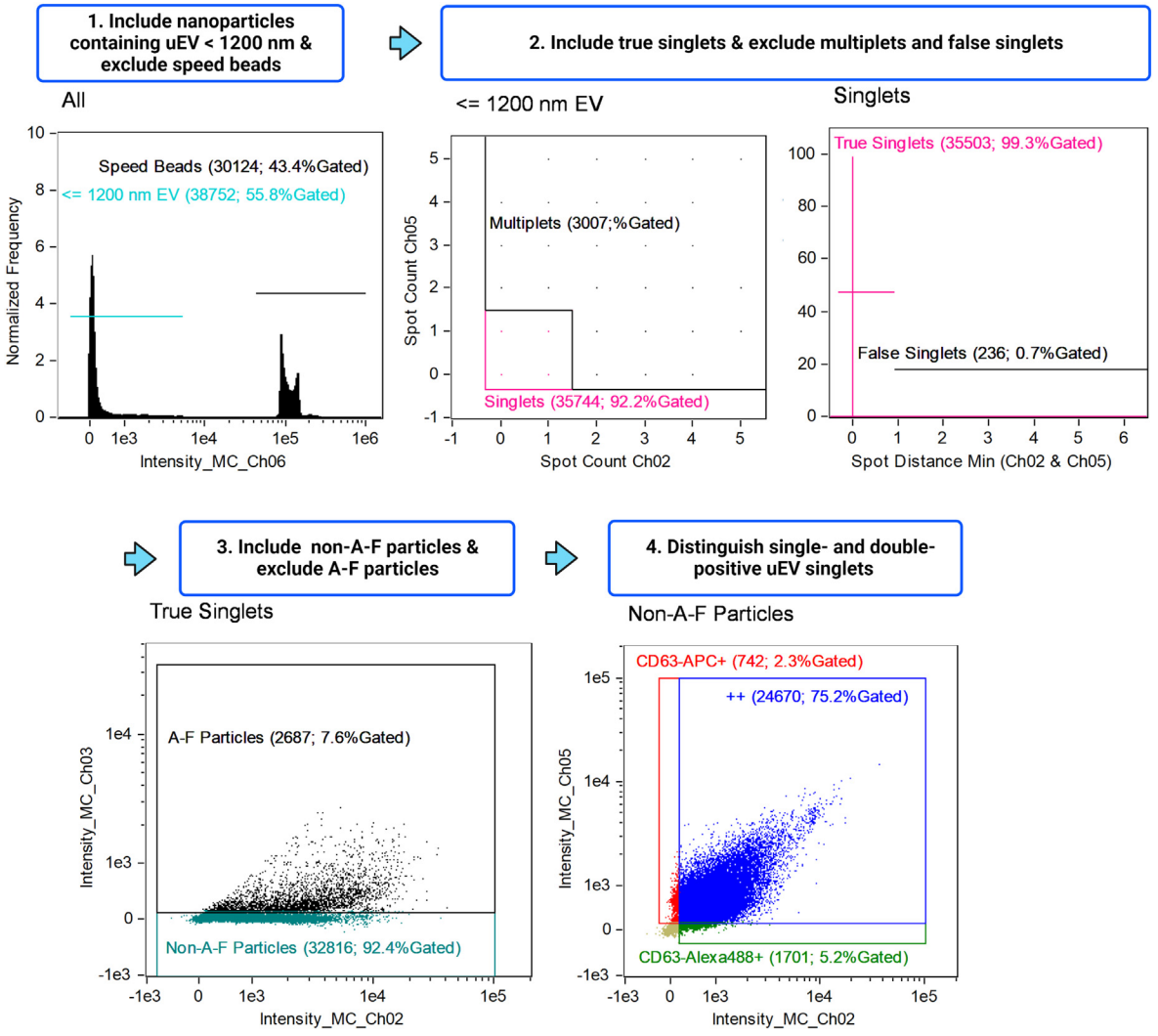

Fig. 4. The final IFCM gating strategy directly identifying CD63+ uEVs in the double-CD63-stained urine. Each gate's name presents the counts and percentage of gated events (Counts; %Gated).

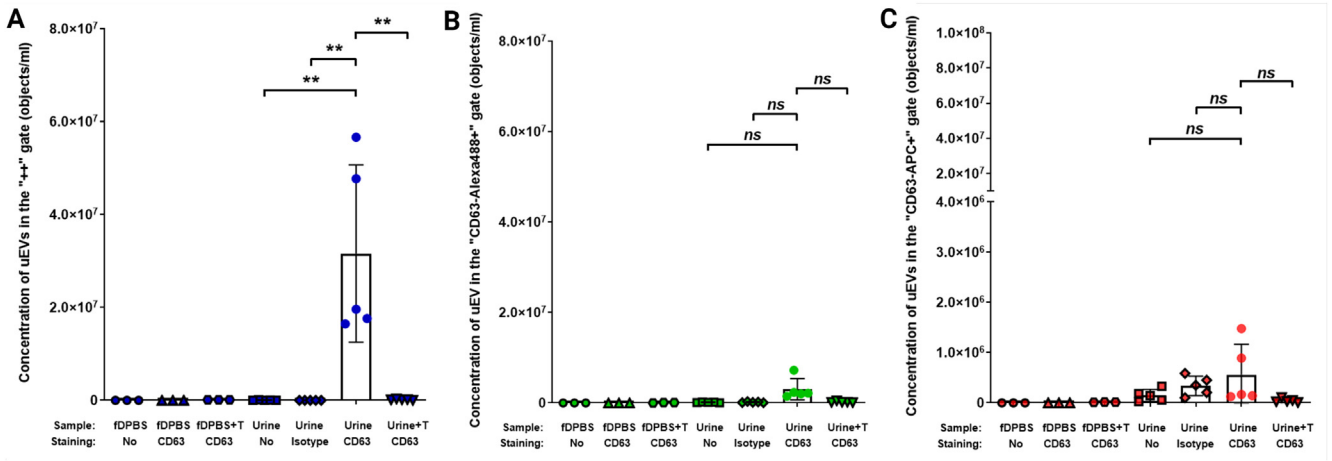

Fig. 5. Verification of the backgrounds and presence of CD63+ uEVs in IFCM. Concentrations of uEVs included in the double-positive gate (++; A), CD63-Alexa488 single-positive gate (B), and CD63-APC single-positive gate (C) negative controls compared with the double-stained healthy urine samples (n = 5). "CD63": staining samples with CD63-Alexa488 and CD63-APC; "Isotype" labeling urine with IgG1-Alexa488 and IgG1-APC; "+T": urine incubated with 0.5 % (v/v) TritonX-100 at room temperature for 30 min. "ns": no significance; $^{**}p < 0.01$.

urine with other treatments, the average uEV-to-background ratios of Alexa488 single-positive and APC single-positive events in the double-stained urine were 10.9-fold and 26.6-fold, respectively (Fig. 5B & C).

Double-positive particles are the majority of CD63+ uEVs and showed the highest uEV-to-background ratio, so they were selected to represent CD63+ uEVs in the subsequent analysis.

Serial dilutions confirm the single-particle analysis

Serial dilutions were performed to verify the detection of single uEVs and the selection of singlets in the IFCM gating strategy.[33] We serially diluted HC urine samples 3- and 9-fold in fDPBS and observed a linear decrease in CD63+ uEV concentration (R^2 = 0.9992; Fig. 6A). This decrease corresponded with the dilution factor, indicating that CD63+ uEVs were single particles.[33] Moreover, diluted samples maintained consistent MESF-Alexa488 and MESF-APC signals of the CD63+ uEVs (Fig. 6B & C). These findings confirmed that our gating strategy correctly identifies and selects single uEVs.

Application and development of the isolation-free protocol for patient's uEV

Our protocol has been developed using HC urine samples and showed good inter- and intra-reproducibility in long-term and repeated measurement for clinical applications (CV < 6.1 %; Supplementary Fig. S7). However, the patient's urine differs from healthy conditions, including higher pH and increased urinary protein levels (Supplementary Table S1). We found that normalizing urinary pH by the commonly used dilution with fDPBS did not alter the detection of uEV numbers (Supplementary Fig. S8). Tamm-Horsfall protein (THP) is the most abundant urinary protein, likely polymerizing and entrapping uEVs, and THP level rises significantly during kidney dysfunctions.[15,16,34]

In election microscopy, unlike most single/free uEVs observed in healthy urine (Supplementary Fig. S2A & B), in the KTR urine, many uEVs are enclosed in aggregate- or filament-like structures (Fig. 7A, large-area pictures in Supplementary Fig. S2C & S2D). These aggregates/filaments might be associated with higher urinary total protein in KTR urine compared with HC urine (p = 0.0050; Fig. 7B). Using ELISA, KTR urine also showed significantly elevated urinary THP compared with HC urine (p = 0.0197; Fig. 7C).

Dithiothreitol (DTT, 200 mg/mL) is a general reagent reducing THP polymerization,[16,35] though excess DTT also breaks the disulfide bond in other molecules, such as present on antibodies.[36] The final concentration of DTT should be carefully considered because there are no washing steps in our protocol. Due to the small sample volume (500 μL) used for each test, reducing the volume of DTT makes it hard to re-suspend the urine pellet, so the concentration of DTT was lowered. Here we used 25 mg/mL and 200 mg/mL DTT to examine the effect of DTT on uEV detection using IFCM.

Compared to the non-DTT group, 25 mg/mL of DTT did not affect CD63+ uEVs concentration in HC urine samples, whereas 200 mg/mL of DTT caused a 9.5 ± 5.2 % decline of detected uEV amounts (p = 0.0431; Fig. 7D). In KTR urine, 25 mg/mL DTT elevated 12.4 ± 10.4 % in CD63+ uEV concentration compared to the non-DTT usage (p = 0.0367; Fig. 7D). However, 200 mg/mL DTT showed a 13.83 ± 3.7 % decrease in uEV numbers compared to the non-DTT group (p = 0.0109; Fig. 7D) in KTR urine. Hence, 25 mg/mL of DTT was used in our developed protocol for applications in patient urine with high levels of THP.

Discussion

We successfully characterized and phenotyped single uEVs in healthy and KTR urine without prior isolation using IFCM in this study.

Our protocol is based on the absolute sizing of EVs with the Mie Theory to realize cross-platform reproducibility.[23,29,37] Conversion of SSC signals into particle size has been demonstrated for our instrument to selectively analyze plasma-derived

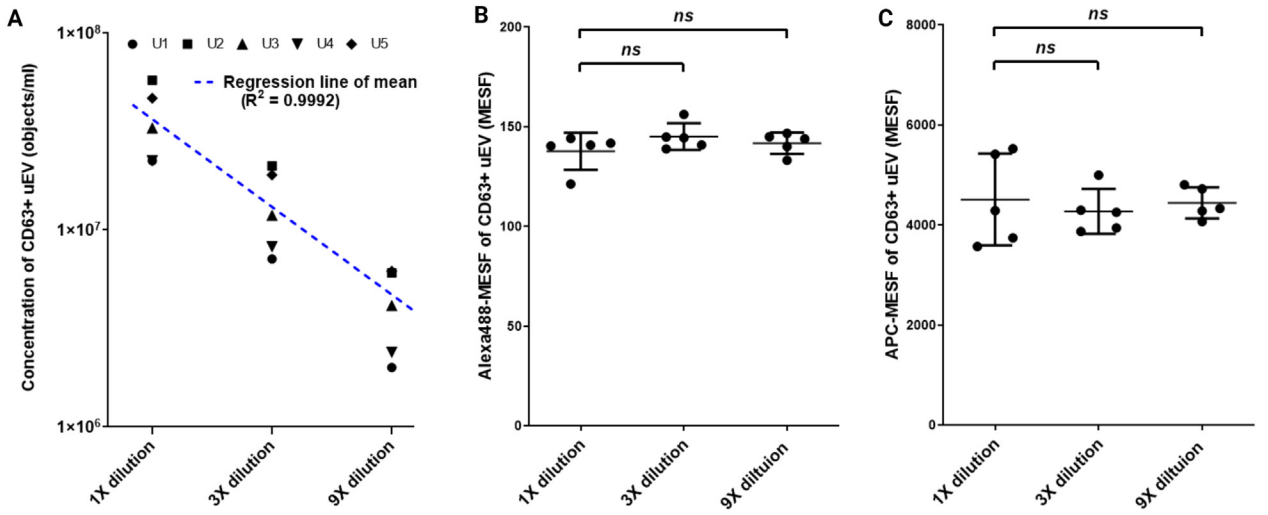

Fig. 6. Verification of uEV singlets in the serially diluted urine. (A) Serial dilutions were performed on the double-stained healthy urine samples (n = 5), showing the linear regression on the mean values of CD63+ uEV concentration. R^2: coefficient of regression. (B, C) Dilution effects on the MESF-Alexa488 and MESF-APC of CD63+ uEV. "ns": no significance.

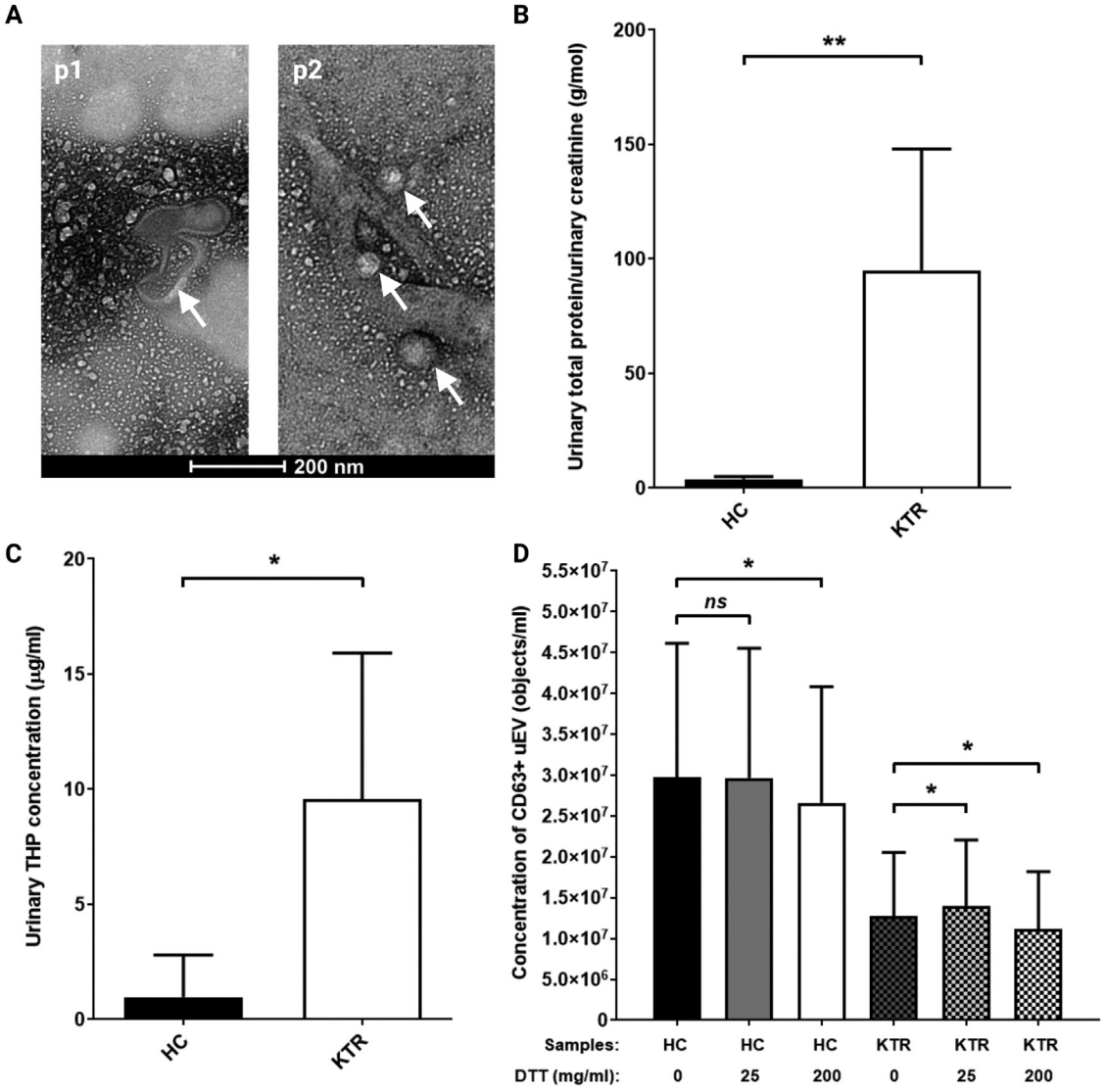

Fig. 7. DTT usage in the IFCM protocol. (A) uEVs in the KTR urine samples measured by TEM. White arrows denoted uEVs. (B, C) The total protein concentrations and THP of HC urine samples (n = 5) and KTR samples (n = 5). $^{**}p < 0.01$; $^{*}p < 0.05$. (D) DTT effects on CD63+ uEV numbers in the HC (n = 5) and KTR urine (n = 5). "ns": no significance; $^{*}p < 0.05$.

EVs ≤400 nm.[23] Here, we expanded the analysis range to investigate uEVs ≤1200 nm because larger uEVs might also be meaningful as a biomarker. Podocytes can release uEVs (≥400 nm) containing abundant RNA and protein markers, serving as an indicator of kidney injury.[14,38] In addition to size, EV shape or membrane orientation might also be of interest, but EV signals with IFCM are indicated with only a few pixels. Therefore other uEV morphology information, such as shape, is challenging to be explored.

This most significant novelty and improvement is the exclusion of urinary A-F particles from uEVs in minimally processed urine. The presence of autofluorescence/A-F particles is a natural property of urine.[14,39] A-F particles presented similar fluorescent characteristics in all the urine samples (HC or KTR). Those particles can be substantially excluded from uEVs with the same gate and compensation matrix (Supplementary Fig. S5), indicating possibly no necessity to adjust the gate or compensation matrix when measuring different urine samples. Following published FCM research,[13,14] we also found that A-F particles in all urine samples showed fluorescence with emission wavelengths 505–595 nm and 642–745 nm. The broad emission wavelength range indicates that A-F particles hinder specific fluorescent EV detection using many typical fluorophores, such as Alexa488, fluorescein isothiocyanate (FITC), PE, Alexa647, and APC. This problem might be avoided by using fluorophores with other emission wavelengths, such as near-infrared ones.[40]

Compared to uEVs, A-F particles might be larger/denser because A-F particles were removed by moderate-speed centrifugation while uEVs were maintained. Large uEVs are co-isolated with A-F particles in the low-centrifugation pellet.[14] Luca et al. tried a masking strategy to delimit A-F in particular channels but observed that 30–40 % of "positive uEVs" remained after detergent lysis.[14] We found that detergent treatment could not entirely remove A-F particles (Fig. 3B), suggesting a

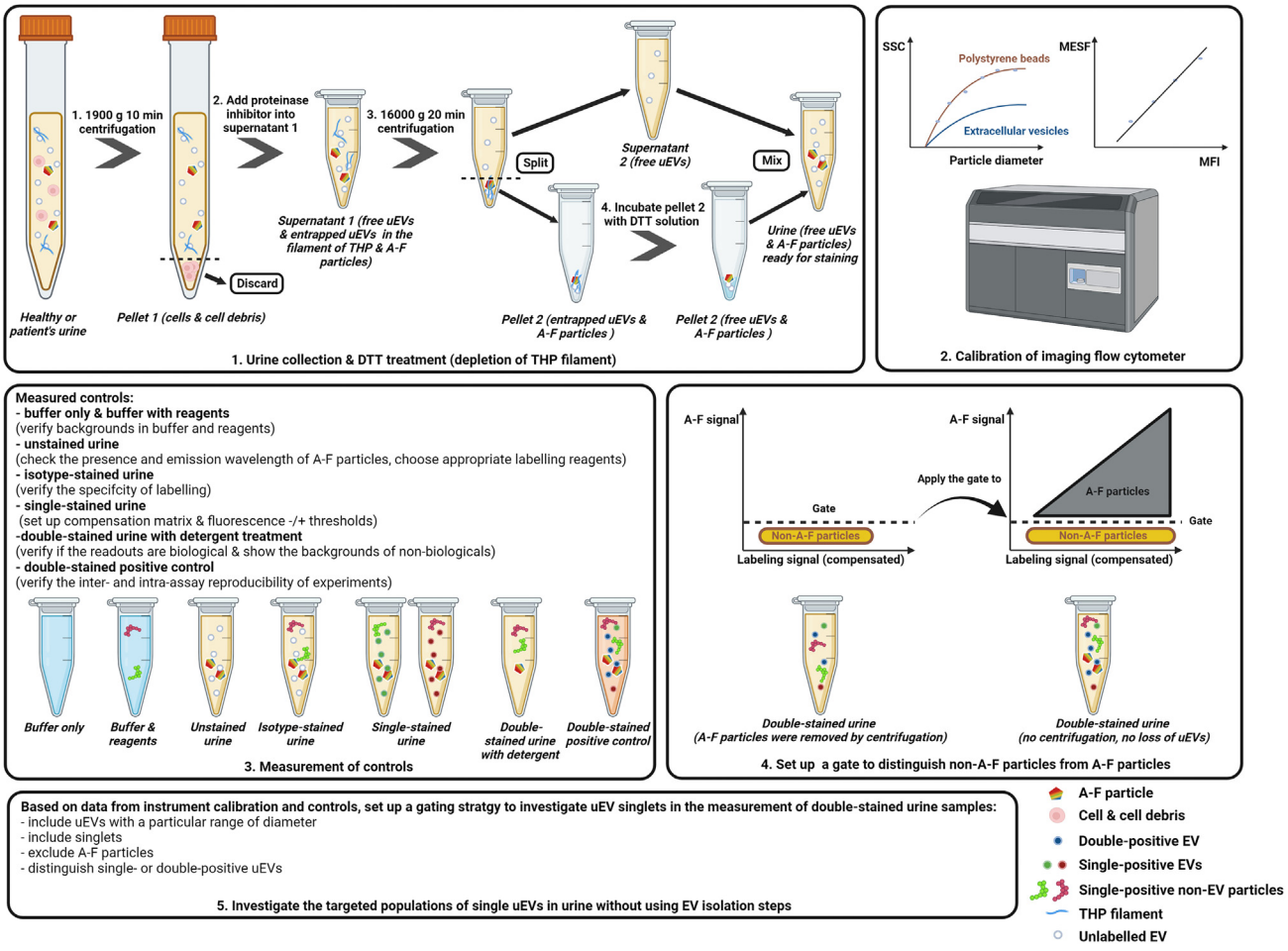

Fig. 8. Schematic summary of the isolation-free protocol measuring uEVs by IFCM.

non-EV structure. We assume A-F particles likely remained in their readouts after their mask strategy. Droste et al. processed urine with a 200 nm filter and did not observe A-F particles using IFCM, but they detected about 10^4 objects/mL CD63+ uEVs.[24] In contrast, in our protocol without filtration, we found around 10^7 objects/mL of CD63+ uEVs. These findings suggest not using filtration or centrifugation when aiming to investigate the full (detectable) spectrum of uEVs.

We chose two CD63 antibodies to demonstrate our methodology. Researchers can easily replace the labeling for detecting other markers but should be cautious in the antibody selection. The single staining with CD63-Alexa488 detected around a 5-fold uEV concentration compared to CD63-APC (Compare Supplementary Fig. S5B with S5C). This finding might be attributed to the fluorophore to protein (F/P) ratio of CD63-Alexa488 (5.20) being much higher than CD63-APC (1.22). A Higher F/P value means brighter fluorescence of each antibody-epitope complex and hence higher sensitivity in the EV detection by FCM.[41]

In this study, we developed our protocol for application in patient samples. During kidney injury, the kidney excretes more THP than in healthy conditions,[34] leading to more entrapment of uEVs.[15] In the patient samples, we found the recovery of uEVs using DTT (10 %) is not as significant as previous reports (20 %),[16,42] which might result from a lower concentration of DTT (25 mg/mL) we used than previous studies (200 mg/mL), because considering the detrimental effects of DTT on antibodies.[36,43]

The limitation of this study is the absence of other quantitative techniques available to compare our IFCM results. However, we do see a correlation between TR-FIA and IFCM (Supplementary Fig. S9A). TR-FIA, independent of isolation, revealed that uEV concentration, not the epitope density on single uEVs, might determine the total uEV protein numbers. Our study met all the requirements of accurate IFCM measurement in the MISEV2018 guideline and MIFlowCyt-EV framework.[1,33] As a method paper, we demonstrate that IFCM is a feasible tool to quantitate and characterize uEVs without bias-concomitant isolation. With our protocol (Fig. 8), uEV researchers can measure targeted subpopulations of uEVs from 500 μL of urine by simply changing the antibody to other markers. More patient urine samples should be enrolled to make the results more robust for clinical application.

Most EV studies relying on isolation used disunited isolation methods, which results in non-comparable data among them. Promoting standardized and isolation-free detection equals

diminishing the research heterogeneity and integrating the data from single-center clinical studies. In conclusion, IFCM provides insight into the differences between single uEVs, A-F particles, and uEV multiplets, allowing for characterizing single uEVs without purification.

CRediT authorship contribution statement

Liang Wu: Methodology, Software, Formal analysis, Investigation, Writing- Original draft preparation, Writing- Reviewing and Editing, Visualization **Wouter W. Woud**: Methodology, Software, Investigation, Writing- Reviewing and Editing **Carla C. Baan**: Resources, Writing- Reviewing and Editing, Supervision, Project administration, Funding acquisition **Dennis A. Hesselink**: Data Curation, Writing- Reviewing and Editing **Edwin van der**: Software, Writing- Reviewing and Editing **Guido Jenster**: Methodology, Writing- Reviewing and Editing **Karin Boer**: Conceptualization, Resources, Data Curation, Writing - Review & Editing, Supervision, Funding acquisition.

Declaration of competing interest

G. Jenster has a license agreement with Cell GS for the CD9 and CD63 TR-FIA (TRIFic). Other author reports no conflicts of interest in this work.

Acknowledgments

We thank the support from the China Scholarship Council (No. 202008430154) and Wenda Verschoor and Rens Kraaijeveld for helping solve the technical questions of IFCM and structure this paper. We acknowledge Natasja Dits at the Department of Urology (Erasmus Medical Center; EMC) for the TEM images and Manou van Alphen for the support of TR-FIA. All figures were created with BioRender.com.

Appendix A. Supplementary data

Supplementary data to this article can be found online at https://doi.org/10.1016/j.nano.2022.102638.

References

1. Théry C, Witwer KW, Aikawa E, Alcaraz MJ, Anderson JD, Andriantsitohaina R, et al. Minimal information for studies of extracellular vesicles 2018 (MISEV2018): a position statement of the International Society for Extracellular Vesicles and update of the MISEV2014 guidelines. *J Extracell Vesicles* 2018;**7**(1):2001-3078, https://doi.org/10.1080/20013078.2018.1535750.
2. Liangsupree T, Multia E, Riekkola ML. Modern isolation and separation techniques for extracellular vesicles. *J Chromatogr A* 2021;**1636**461773, https://doi.org/10.1016/j.chroma.2020.461773.
3. Arraud N, Linares R, Tan S, Gounou C, Pasquet JM, Mornet S, et al. Extracellular vesicles from blood plasma: determination of their morphology, size, phenotype and concentration. *J Thromb Haemost* 2014;**12**(5):614-27, https://doi.org/10.1111/JTH.12554.
4. Wen J, Yang T, Mallouk N, Zhang Y, Li H, Lambert C, et al. Urinary exosomal CA9 mRNA as a novel liquid biopsy for molecular diagnosis of bladder cancer. *Int J Nanomedicine* 2021;**16**:4805-11, https://doi.org/10.2147/IJN.S312322.
5. Wu L, Boer K, Woud WW, Udomkarnjananun S, Hesselink DA, Baan CC. Urinary extracellular vesicles are a novel tool to monitor allograft function in kidney transplantation: a systematic review. *Int J Mol Sci* 2021;**22**(19):10499, https://doi.org/10.3390/ijms221910499.
6. Liu YR, Ortiz-Bonilla CJ, Lee YF. Extracellular vesicles in bladder cancer: biomarkers and beyond. *Int J Mol Sci* 2018;**19**(9), https://doi.org/10.3390/IJMS19092822.
7. Kamińska A, Roman M, Wróbel A, Gala-Błądzińska A, Małecki MT, Paluszkiewicz C, et al. Raman spectroscopy of urinary extracellular vesicles to stratify patients with chronic kidney disease in type 2 diabetes. *Nanomed Nanotechnol Biol Med* 2022;**39**102468, https://doi.org/10.1016/J.NANO.2021.102468.
8. Wang S, Kojima K, Mobley JA, West AB. Proteomic analysis of urinary extracellular vesicles reveal biomarkers for neurologic disease. *EBioMedicine* 2019;**45**:351-61, https://doi.org/10.1016/j.ebiom.2019.06.021.
9. Gonzalez E, Azkargorta M, Garcia-Vallicrosa C, Prieto-Elordui J, Elortza F, Blanco-Sampascual S, et al. Could protein content of urinary extracellular vesicles be useful to detect cirrhosis in alcoholic liver disease? *Int J Biol Sci* 2021;**17**(8):1864-77, https://doi.org/10.7150/IJBS.59725.
10. Erdbrügger U, Blijdorp CJ, Bijnsdorp IV, Borràs FE, Burger D, Bussolati B, et al. Urinary extracellular vesicles: a position paper by the urine task force of the International Society for Extracellular Vesicles. *J Extracell Vesicles* 2021;**10**(7)e12093, https://doi.org/10.1002/jev2.12093.
11. Cimorelli M, Nieuwland R, Varga Z, van der Pol E. Standardized procedure to measure the size distribution of extracellular vesicles together with other particles in biofluids with microfluidic resistive pulse sensing. *PLoS One* 2021;**16**(4), https://doi.org/10.1371/JOURNAL.PONE.0249603.
12. van der Pol E, Sturk A, van Leeuwen T, Nieuwland R, Coumans F, Mobarrez F, et al. Standardization of extracellular vesicle measurements by flow cytometry through vesicle diameter approximation. *J Thromb Haemost* 2018;**16**(6):1236-45, https://doi.org/10.1111/jth.14009.
13. Burger D, Thibodeau JF, Holterman CE, Burns KD, Touyz RM, Kennedy CRJ. Urinary podocyte microparticles identify prealbuminuric diabetic glomerular injury. *J Am Soc Nephrol* 2014;**25**(7):1401-7, https://doi.org/10.1681/ASN.2013070763.
14. Musante L, Bontha SV, La Salvia S, Fernandez-Piñeros A, Lannigan J, Le TH, et al. Rigorous characterization of urinary extracellular vesicles (uEVs) in the low centrifugation pellet - a neglected source for uEVs. *Sci Rep* 2020;**10**(1):1-14, https://doi.org/10.1038/s41598-020-60619-w.
15. Xu X, Barreiro K, Musante L, Kretz O, Lin H, Zou H, et al. Management of Tamm-Horsfall Protein for reliable urinary analytics. *Proteomics - Clin Appl* 2019;**13**(6):1-10, https://doi.org/10.1002/prca.201900018.
16. Fernández-Llama P, Khositseth S, Gonzales PA, Star RA, Pisitkun T, Knepper MA. Tamm-horsfall protein and urinary exosome isolation. *Kidney Int* 2010;**77**(8):736-42, https://doi.org/10.1038/ki.2009.550.
17. Stam J, Bartel S, Bischoff R, Wolters JC. Isolation of extracellular vesicles with combined enrichment methods. *J Chromatogr B Anal Technol Biomed Life Sci* 2021:1169, https://doi.org/10.1016/j.jchromb.2021.122604.
18. Jang SC, Kim OY, Yoon CM, Choi DS, Roh TY, Park J, et al. Bioinspired exosome-mimetic nanovesicles for targeted delivery of chemotherapeutics to malignant tumors. *ACS Nano* 2013;**7**(9):7698-710, https://doi.org/10.1021/nn402232g.
19. Pang B, Zhu Y, Ni J, Ruan J, Thompson J, Malouf D, et al. Quality assessment and comparison of plasma-derived extracellular vesicles separated by three commercial kits for prostate cancer diagnosis. *Int J Nanomedicine* 2020;**15**:10241-56, https://doi.org/10.2147/IJN.S283106.
20. Linares R, Tan S, Gounou C, Arraud N, Brisson AR. High-speed centrifugation induces aggregation of extracellular vesicles. *J Extracell Vesicles* 2015;**4**(1), https://doi.org/10.3402/jev.v4.29509.
21. Botha J, Pugsley HR, Handberg A. Conventional, high-resolution and imaging flow cytometry: benchmarking performance in characterisation of extracellular vesicles. *Biomedicines* 2021;**9**(2):1-24, https://doi.org/10.3390/biomedicines9020124.

22. Görgens A, Bremer M, Ferrer-Tur R, Murke F, Tertel T, Horn PA, et al. Optimisation of imaging flow cytometry for the analysis of single extracellular vesicles by using fluorescence-tagged vesicles as biological reference material. *J Extracell Vesicles* 2019;**8**(1):1587567, https://doi.org/10.1080/20013078.2019.1587567.
23. Woud WW, van der Pol E, Mul E, Hoogduijn MJ, Baan CC, Boer K, et al. An imaging flow cytometry-based methodology for the analysis of single extracellular vesicles in unprocessed human plasma. *Commun Biol* 2022;**40**(1):633, https://doi.org/10.1101/2022.02.24.481807.
24. Droste M, Tertel T, Jeruschke S, Dittrich R, Kontopoulou E, Walkenfort B, et al. Single extracellular vesicle analysis performed by imaging flow cytometry and nanoparticle tracking analysis evaluate the accuracy of urinary extracellular vesicle preparation techniques differently. *Int J Mol Sci Artic Int J Mol Sci* 2021;**22**(22):12436, https://doi.org/10.3390/ijms222212436.
25. Lannigan J, Erdbruegger U. Imaging flow cytometry for the characterization of extracellular vesicles. *Methods* 2017;**112**:55-67, https://doi.org/10.1016/j.ymeth.2016.09.018.
26. M Mathieu N Névo M Jouve JI Valenzuela M Maurin FJ Verweij et alSpecificities of exosome versus small ectosome secretion revealed by live intracellular tracking of CD63 and CD9. doi:10.1038/s41467-021-24384-2
27. Royo F, Zuñiga-Garcia P, Sanchez-Mosquera P, Egia A, Perez A, Loizaga A, et al. Different EV enrichment methods suitable for clinical settings yield different subpopulations of urinary extracellular vesicles from human samples. *J Extracell Vesicles* 2016;**5**(1), https://doi.org/10.3402/jev.v5.29497.
28. Amnis. *IDEAS® Image Data Exploration and Analysis Software User's Manual*, July. ; 2013. p. 231https://www.luminexcorp.com/imagestreamx-mk-ii/?wpdmdl=41965.
29. de Rond L, Coumans FAW, Nieuwland R, van Leeuwen TG, van der Pol E. Deriving extracellular vesicle size from scatter intensities measured by flow cytometry. *Curr Protoc Cytom* 2018;**86**(1)e43, https://doi.org/10.1002/cpcy.43.
30. Van Deun J, Mestdagh P, Agostinis P, Akay Ö, Anand S, Anckaert J, et al. EV-TRACK: transparent reporting and centralizing knowledge in extracellular vesicle research. *Nat Methods* 2017 143. 2017;**14**(3):228-32, https://doi.org/10.1038/nmeth.4185.
31. van der Pol E, Coumans FAW, Grootemaat AE, Gardiner C, Sargent IL, Harrison P, et al. Particle size distribution of exosomes and microvesicles determined by transmission electron microscopy, flow cytometry, nanoparticle tracking analysis, and resistive pulse sensing. *J Thromb Haemost* 2014;**12**(7):1182-92, https://doi.org/10.1111/jth.12602.
32. Duijvesz D, Versluis CYL, Van Der Fels CAM, Vredenbregt-Van Den Berg MS, Leivo J, Peltola MT, et al. Immuno-based detection of extracellular vesicles in urine as diagnostic marker for prostate cancer. *Int J Cancer* 2015;**137**(12):2869-78, https://doi.org/10.1002/ijc.29664.
33. Welsh JA, Van Der Pol E, Arkesteijn GJA, Bremer M, Brisson A, Coumans F, et al. MIFlowCyt-EV: a framework for standardized reporting of extracellular vesicle flow cytometry experiments. *J Extracell Vesicles* 2020;**9**(1), https://doi.org/10.1080/20013078.2020.1713526.
34. Rampoldi L, Scolari F, Amoroso A, Ghiggeri G, Devuyst O. The rediscovery of uromodulin (Tamm-horsfall protein): from tubulointerstitial nephropathy to chronic kidney disease. *Kidney Int* 2011;**80**(4):338-47, https://doi.org/10.1038/ki.2011.134.
35. Lozano-Ramos I, Bancu I, Oliveira-Tercero A, Armengol MP, Menezes-Neto A, Del Portillo HA, et al. Size-exclusion chromatography-based enrichment of extracellular vesicles from urine samples. *J Extracell Vesicles* 2015;**2015**(4):1-11, https://doi.org/10.3402/jev.v4.27369.
36. Crivianu-Gaita V, Romaschin A, Thompson M. High efficiency reduction capability for the formation of Fab' antibody fragments from F(ab)2 units. *Biochem Biophys Rep* 2015;**2**:23-8, https://doi.org/10.1016/j.bbrep.2015.04.004.
37. van der Pol E, de Rond L, Coumans FAW, Gool EL, Böing AN, Sturk A, et al. Absolute sizing and label-free identification of extracellular vesicles by flow cytometry. *Nanomed Nanotechnol Biol Med* 2018;**14**(3):801-10, https://doi.org/10.1016/j.nano.2017.12.012.
38. Liu Y, Li S, Rong W, Zeng C, Zhu X, Chen Q, et al. Podocyte-released migrasomes in urine serve as an indicator for early podocyte injury. *Kidney Dis (Basel, Switzerland)* 2020;**6**(6):422-33, https://doi.org/10.1159/000511504.
39. Birková A, Oboril J, Kréta R, Čižmárová B, Hubková B, Šteffeková Z, et al. Human fluorescent profile of urine as a simple tool of mining in data from autofluorescence spectroscopy. *Biomed Signal Process Control* 2020;**56**101693, https://doi.org/10.1016/J.BSPC.2019.101693.
40. Hong G, Antaris AL, Dai H. Near-infrared fluorophores for biomedical imaging. *Nat Biomed Eng* 2017;**1**(1):1-22, https://doi.org/10.1038/s41551-016-0010.
41. Gankema AAF, Li B, Nieuwland R, van der Pol E. Automated fluorescence gating and size determination reduce variation in measured concentration of extracellular vesicles by flow cytometry. *Cytom Part A* 2022, https://doi.org/10.1002/cyto.a.24665.
42. Correll VL, Otto JJ, Risi CM, Main BP, Boutros PC, Kislinger T, et al. Optimization of small extracellular vesicle isolation from expressed prostatic secretions in urine for in-depth proteomic analysis. *J Extracell Vesicles* 2022;**11**(2), https://doi.org/10.1002/jev2.12184.
43. Li Y, Nese A, Lebedeva NV, Davis T, Matyjaszewski K, Sheiko SS. Molecular tensile machines: intrinsic acceleration of disulfide reduction by dithiothreitol. *J Am Chem Soc* 2011;**133**(43):17479-84, https://doi.org/10.1021/ja207491r.